https://doi.org/10.1007/s41230-024-3083-0

Effect of Sc on Al_3Fe phase and mechanical properties of as-cast AA5052 aluminum alloy

Yang Li, Qing Yu, Feng-feng Chen, Jia-wen He, *Hong-mei Yang, and **Meng-nie Li

Faculty of Materials Science and Engineering, Kunming University of Science and Technology, Kunming 650093, China

Abstract: The AA5052 aluminum alloy is widely used in automobile and aerospace manufacturing, and with the development of light-weight alloys, it is required that these materials exhibit better mechanical properties. Previous studies have demonstrated that the addition of Sc to aluminum alloys can improve both the microstructure and properties of the alloys. In this study, the effect of Sc on the Fe-rich phase and properties of the AA5052 aluminum alloy was studied by adding 0%, 0.05%, 0.2%, and 0.3% Sc. The results show that with the increase of Sc, the coarse needle-like Fe-rich phase gradually transforms into Chinese-script and then nearly spherical particles, reduce the size of Fe-rich phase, and refine the grain with increase of high angle grain boundaries (HAGBs). These microstructure changes enhance the strength of the AA5052 alloy through Sc addition. The ductility of the alloy is obviously improved because the addition of a lower amount of Sc changes the morphology of Fe-rich phase from needle-like into a Chinese-script, and it is subsequently reduced as a result of significant increase in HAGBs with increasing Sc content.

Keywords: AA5052 aluminum alloy; Al_3Fe phase; mechanical properties; grain boundary

CLC numbers: TG146.21 **Document code:** A **Article ID:** 1672-6421(2024)03-257-08

1 Introduction

The AA5052 aluminum alloy is widely used in aircraft fuel tanks, automobiles, marine vessels, and construction industries due to its excellent properties, such as light weight, medium strength, good corrosion resistant, good weldability, and easy to process [1-5]. With the continuous development of aerospace and other new technologies, AA5052 aluminum alloys with better performance are required, which is improved by optimizing the microstructure. For AA5052 aluminum alloys, the secondary phases include Mg_2Si and Al_3Fe, which are unchanged after subsequent processing [6]. In aluminum alloys, Fe is a common impurity, which forms an Fe-rich phase with a strip- or plat-shape. The coarse Fe-rich phase easily acts as crack source and reduces the performance of aluminum alloys during heat treatment and rolling [7]. The brittle Fe-rich phase forms in low Fe content environments and its morphology and size have a significant effect on the mechanical properties of aluminum parts. The method of microalloying is one of the effective means to improve Fe-rich phase morphology to obtain high strength, high toughness, and good corrosion resistance [8-13]. Furthermore, adding neutralizing elements, such as Mn and Si, can modify the sharp morphologies of Fe phases to decrease damage [14].

Recently, a significant amount of literatures have reported that the addition of Sc to aluminum alloys have a positive effect on the microstructure and properties of the alloy [15-19]. Tang et al. [20] used Sc to modify the 6066 aluminum alloy and found that as the content of Sc increased from 0% to 0.2%, the average grain size of alloy ingots decreased from 45 μm to 20 μm, and the microstructural homogeneity was also improved. The strong grain refining effect on aluminum alloys can also improve their casting structure. Li et al. [21] found that with increasing Sc content, the microstructure of Al-Zn-Mg-Zr alloy also gradually changed from dendrite to equiaxed crystalline. Wang et al. [22] found that adding Sc and Ti to sand-cast Al-Li-Cu-Mg-Zr alloy effectively decreased the grain size from 189 μm to 56 μm. The mechanism of Sc grain refinement is that Sc reacts with Al to form Al_3Sc particles. These particles have an $L1_2$

***Hong-mei Yang**

Female, Ph. D. Professor. Research interests: high pressure die casting and semi-continuous casting of Al and Cu alloys, and microstructure simulation during solidification.

E-mail: yhmei125@kust.edu.cn

****Meng-nie Li**

E-mail: limengnie@kust.edu.cn

Received: 2023-08-28; Accepted: 2024-02-02

structure and act as heterogeneous nuclei. The Al_3Sc has a FCC crystal structure similar to α-Al. The lattice parameter of Al_3Sc is 0.4106 nm, which is close to α-Al, which is 0.405 nm. The match between them is closer than for any other known grain refining nuclei used in Al alloys, and the Al_3Sc particles can grow on all primary aluminum crystal planes [23, 24]. Therefore, Sc is one of the most effective primitives for grain refinement in aluminum alloys, and it outperforms most other elements [25]. Recent studies have focused on the effects of adding Sc to 5xxx aluminum alloys with Mg≥3.5wt.% [2, 4, 10]. However, few studies on adding Sc to low-Mg 5052 aluminum alloy.

In this study, four different groups of AA5052 aluminum alloys were prepared by adding Sc. The Al_3Fe phase of the alloy was micro-characterized by scanning electron microscopy (SEM), the grain sizes of the alloy were statistically calculated by EBSD, and the grain boundary characteristics were analyzed. A room temperature tensile test was applied with a universal testing machine to investigate the influence of Sc on mechanical properties of the 5052 aluminum alloy, which was expected to provide a theoretical and experimental basis for the development of a new high-strength Al-Mg-Sc-Zr alloy.

2 Experiment and method

Pure aluminum (99.99wt.%), pure magnesium (99.99wt.%), Al-10wt.% Mn, Al-20wt.% Si, Al-50wt.% Cr, Al-10wt.% Fe, Cu-50wt.% Zn, and Al-2wt.% Sc master alloys were used to prepare the AA5052 aluminum alloy samples with different concentrations of Sc (0.00wt.%, 0.05wt.%, 0.20wt.%, and 0.30wt.%). The casting process was as follows: (1) Melted pure Al in a vacuum induction furnace at 760 °C; (2) Added a suitable quantity of master alloys in the order of Al-10wt.% Mn and Al-20wt.% Si, Al-50wt.% Cr, Al-10wt.% Fe, and Cu-50wt.% Zn, and held for 5 min after each addition; (3) Added a corresponding concentration of Al-2wt.% Sc master alloys at 730 °C, and held for 10 min, then added pure magnesium and held for 5 min; (4) Reduced the temperature to 710 °C and poured the melt into a water-cooled permanent mold (with the dimensions of 120 mm×50 mm×50 mm) to obtain the experimental cast alloys. The composition of the experimental alloys was determined by a direct current plasma-optical emission spectrometer (DCP-OES), as presented in Table 1.

Table 1: Composition of aluminum alloy samples (wt.%)

Alloy	Si	Fe	Mg	Cu	Zn	Mn	Cr	Sc	Al
1	0.082	0.275	2.710	0.095	0.964	0.096	0.110	0.000	Bal.
2	0.102	0.355	2.410	0.082	0.101	0.095	0.106	0.050	Bal.
3	0.087	0.348	2.380	0.103	0.110	0.095	0.080	0.200	Bal.
4	0.098	0.372	2.480	0.114	0.104	0.100	0.088	0.297	Bal.

The samples used for microstructure observation were machined from cast ingots. All samples were mechanically ground and deeply etched with a solution of Keller reagent (2.5 mL HNO_3+1.0 mL HF+1.5 mL HCl+95 mL H_2O) for 15 s. Microstructure observation including the second phase composition analysis was then characterized by a tungsten filament scanning electron microscope (SEM, VEGA3 TESCAN) with an energy dispersive X-ray spectrometer (EDS). A JSM7200F JEOL field emission scanning electron microscope (FE-SEM) equipped with an electron back-scatter diffraction (EBSD, JSM 7200F) system was utilized for EBSD analysis, including grain size and misorientation angle quantification. The data were analyzed using Channel 5 analysis software provided by Oxford HKL Technology. The step size was 0.5 μm under an accelerating voltage of 20 kV. The scan area was 1×1 mm^2 for the average grain size analysis and 500×500 μm^2 for the misorientation angle quantification. The misorientation angle quantification was used to determine low angle grain boundaries (LAGBs, between 2° and 15°) and high angle grain boundaries (HAGBs, above 15°). In the IPF diagram of the EBSD maps, the black and red lines indicate the HAGBs and LAGBs, respectively. The Al_3Fe and Mg_2Si phases were characterized by transmission electron microscopy (TEM, FEI Tecnai G2 F20).

All tensile specimens were machined from ingots according to the schematic shown in Fig. 1. The mechanical property analysis was performed on a Shimadzu Electronic Universal Material Testing Machine (AG-X Plus) at room temperature with a tensile speed of 0.6 mm·min^{-1}.

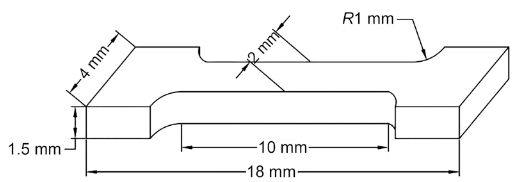

Fig. 1: Schematic of the tensile specimen

3 Results and discussion

3.1 Microstructure analysis

Figure 2 shows the typical second phases of as-cast AA5052 alloy without Sc. EDS results in Table 2 indicate the black and white phases are Al_3Fe and Mg_2Si, respectively. Figure 3 shows the SEM image of as-cast AA5052 alloy with and without Sc. The Al_3Fe phase in the as-cast AA5052 alloy without Sc exhibits a coarse needle-like shape in the grain boundaries, and most of the phases exhibit a strip shape with a length above 100 μm, as shown in Fig. 3(a). It finds that the addition of Sc in AA5052

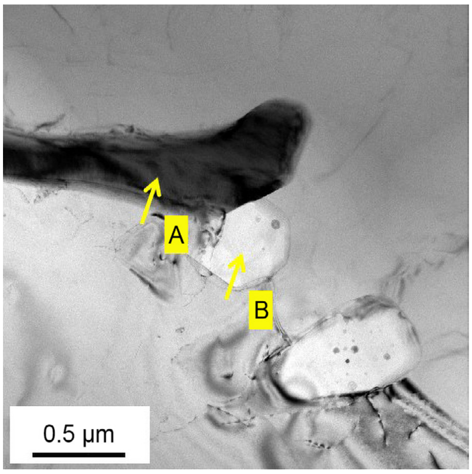

Fig. 2: Typical second phases of as-cast AA5052 alloy

alloy changes the morphology of the Al_3Fe phase [Figs. 3(b–d)]. With the addition of 0.05wt.% Sc in AA5052 alloy, the morphology of Al_3Fe phase transforms from coarse needle-like into Chinese-script with a length less than 10 μm [Fig. 3(b)]. Upon further increasing the Sc content to 0.2wt.%, the Chinese-script Al_3Fe phase changes to short rod-like with an average length of 5.5 μm [Fig. 3(c)]. When the Sc concentration is 0.3wt.%, the vast majority of the Al_3Fe phase exhibits a near-spherical shape with about 2 μm in size ([Fig. 3(d)]. The results indicate that the addition of Sc can inhibit the growth of the corase needle-like Al_3Fe phase and leading to a more refined Al_3Fe phase in AA5052 alloy.

Figure 4 shows EBSD maps for Alloys 1, 2, 3, and 4. The grains of the AA5052 aluminum alloy without Sc are relatively coarse, and the average grain size is about 138 μm, as shown in Fig. 4(a). With the addition of Sc to AA5052 aluminum alloy, the average grain sizes of Alloys 2, 3, and 4 with different Sc concentrations are 74 μm, 64 μm, and 40 μm, respectively [Figs. 4(b–d)]. This indicates that the addition of Sc has a significant grain refinement effect. Figure 5 shows a TEM image of Alloy 4. Each black spot in the TEM image is a column of Sc-rich atoms, which can be identified as an Al_3Sc precipitate by diffraction spots. The Al_3Sc particles act as heterogeneous nuclei, which refine the primary α-Al [23].

Figure 6 shows the selected IPF plots of EBSD observation. The EBSD observation range of Alloy 1 was selected to be 1 mm×1 mm and the step size was set to 2 μm. The observation range of the Alloys 2–4 was selected to be 500 μm×500 μm and the step size was set to 1 μm. The grain boundary is superimposed on the IPF diagram: black represents the high angle grain boundaries (HAGBs) above 15°, and red represents the low angle grain boundaries (LAGBs) between 2°–15°. The proportion of low angle grain boundaries in Alloy 1 reaches 69.5%, in Alloy 2 reaches 67.5%, in Alloy 3 reaches 61.8%, and in Alloy 4 reaches 57.4%. The proportion of HAGBs is 26.8%, 27.2%, 34.3%, and 39.8% in Alloys 1, 2, 3 and 4, respectively. It is obvious that the LAGBs proportion decreases and correspondingly HAGBs increases with increasing the concentration of Sc. This difference is likely to eventually lead to a difference in the strength of the material.

Table 2: EDS results of phases indicated by arrows in Fig. 2 (at.%)

Phase	Al	Fe	Si	Cu	Zn	Mn	Cr	Mg
A	73.53	23.67	0.94	0.14	0	0.01	0.14	1.57
B	2.86	0.57	33.31	0	0.02	0.1	0.12	63.02

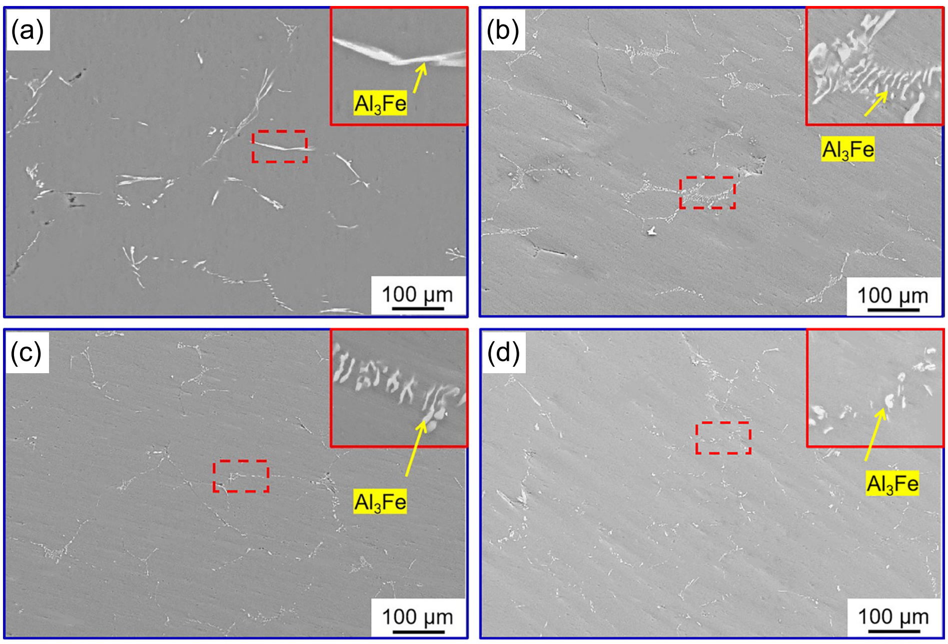

Fig. 3: Scattered SEM micrographs of the Al_3Fe phase: (a) Alloy 1; (b) Alloy 2; (c) Alloy 3; (d) Alloy 4

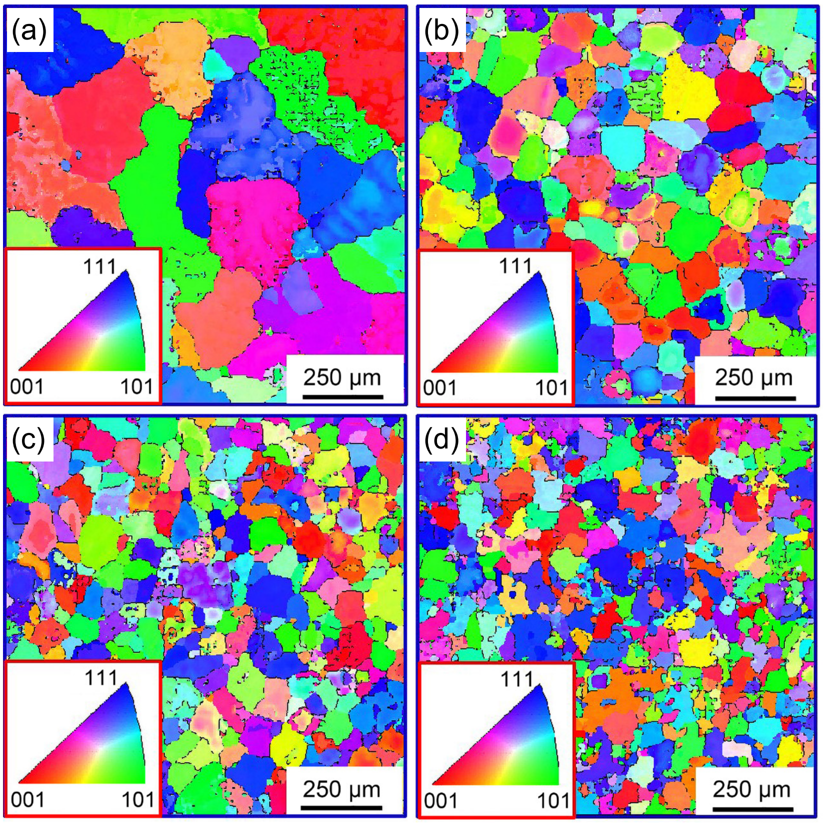

Fig. 4: EBSD maps for alloys with different contents of Sc: (a) Alloy 1; (b) Alloy 2; (c) Alloy 3; (d) Alloy 4

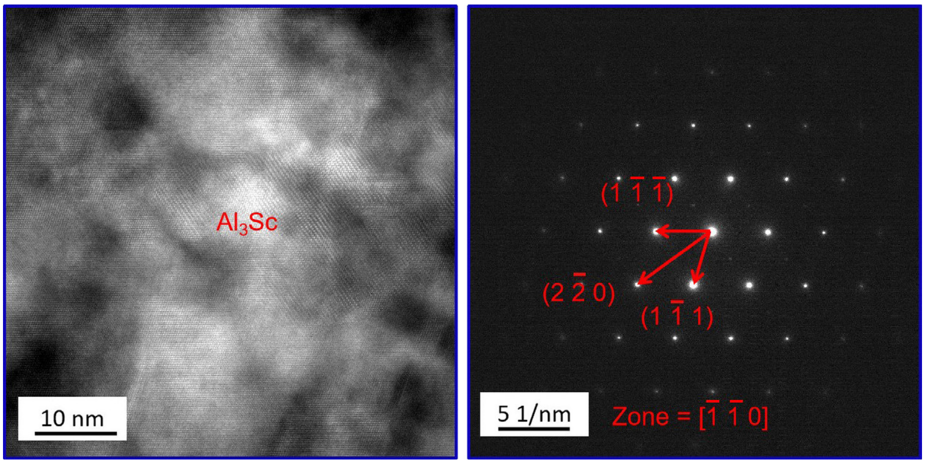

Fig. 5: TEM map of Al_3Sc particles in Alloy 4

3.2 Mechanical properties

Figure 7 shows the stress-strain curves and the average tensile strength and elongation of the four groups of aluminum alloys. When Sc concentration is 0wt.%, the ultimate tensile strength of the alloy is 181.3 MPa and the elongation is 19.8%. When the Sc concentration increases to 0.05wt.%, the ultimate tensile strength is 196.3 MPa and the elongation increases to 30%. When Sc concentration increases to 0.2wt.%, the ultimate tensile strength increases to 216 MPa and the elongation decreases to 23.5%. When Sc concentration is further increased to 0.3wt.%, the ultimate tensile strength is 251 MPa and the elongation is 19.3%. Thus, it can be deduced that the ultimate tensile strength of the alloy increases with increasing Sc concentration, while the elongation shows a trend of firstly increase and then decrease. The increase in ultimate tensile strength can be attributed to several factors. The first is that the addition of Sc changes the morphology of Al_3Fe phase and reduces its harmful effect. The second is the effect of grain refinement. As suggested by the theory of non-uniform nucleation, the degree of refinement of the grain depends on the number of nucleation particles in the melt and the effective nucleation of the particles. Among them, the effective nucleation of particles depends on the lattice constant and the lattice type of the nucleation particles and the α-Al matrix [26]. The Al_3Sc particles precipitated by Sc in the alloy melt have an $L1_2$-type face-centered cubic lattice, which act

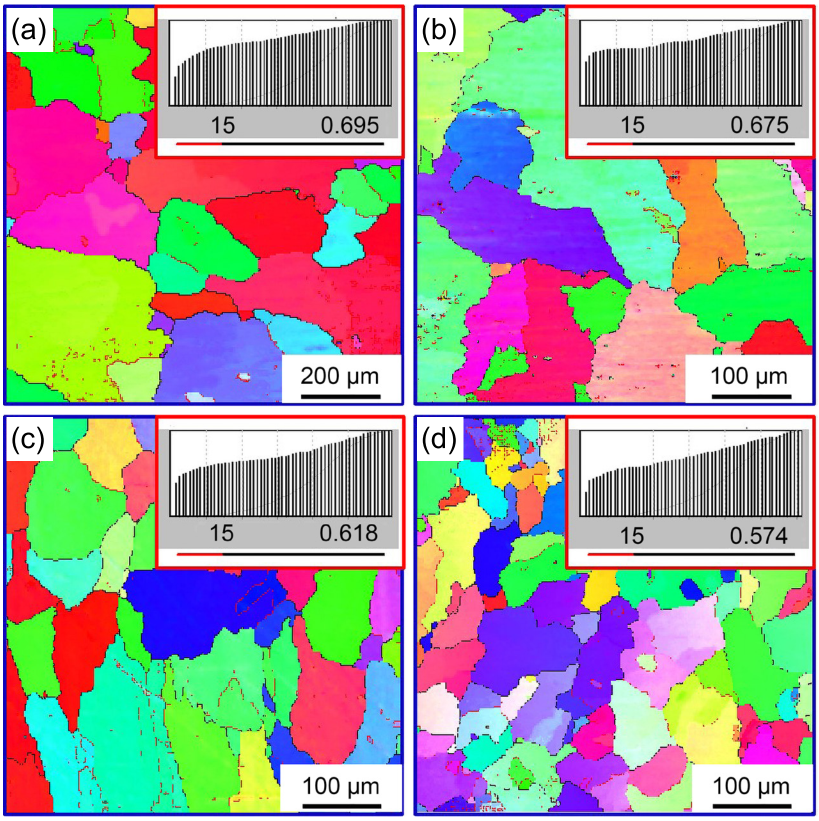

Fig. 6: Selected IPF plots of the EBSD maps of Alloy 1 (a), Alloy 2 (b), Alloy 3 (c), and Alloy 4 (d)

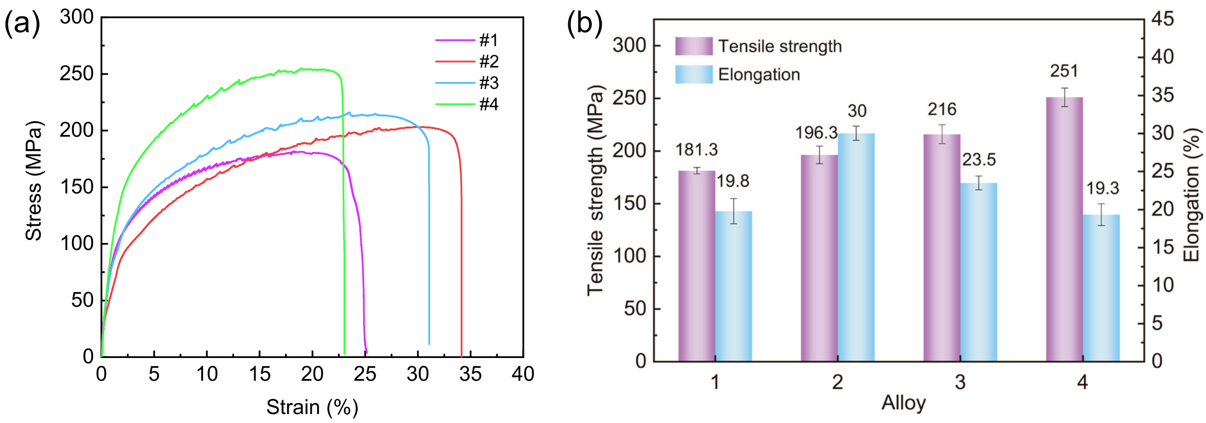

Fig. 7: Stress-strain curves of alloys with different Sc concentrations (a) and average tensile strength and elongation of alloys with different Sc concentrations (b)

as the high-quality heterogeneous nuclei of α-Al in the alloy solidification process, effectively refining the aluminum matrix grains [23]. Moreover, the LAGBs decrease with the increase of Sc. The LAGBs are formed by a dislocation motion, and these dislocations gradually accumulate, resulting in the gradual increase of the orientation difference of the grains on both sides [27]. Compared with the HAGBs, the LAGBs boundary can be more easily broken when the dislocation moves near the LAGBs boundary due to the small orientation difference between adjacent grain boundaries, rather than accumulating at the grain boundary, which is a common occurrence at HAGBs. The accumulation of dislocations at HAGBs leads to a concentration of stress [28]. This observation suggests that the strength of the alloy is enhanced by the increase of HAGBs, which can inhibit the movement of dislocations. With the further increase of HAGBs, the defects at the grain boundaries increase and the plasticity of the material decreases.

3.3 Fracture morphology

Figure 8 shows the tensile fracture morphology of the alloys with different Sc contents. The presence of dimples in the fracture of all the four alloys indicates a ductile fracture. For Alloy 1 without Sc, the long-strip Al_3Fe phase is observed at the intersection of the tearing ridges, as shown in Fig. 8(a). This indicates that in the process of tensile deformation, microcracks are generated around the Al_3Fe phase, and the micropores extend along the interface between the matrix and the Al_3Fe phase, forming large cracks around the phase. The rapid expansion of the cracks then leads to the failure of the alloy. Whereas the Al_3Fe phases present at the bottom of the dimple pit of alloys with addition of Sc contents, as shown in Figs. 8(b), (c) and (d). When the morphology of Al_3Fe phase changes from coarse needle-like to Chinese-script, the ductility is significantly improved, such as Alloys 2 and 3 of the Sc-containing alloys. When the content of Sc is increased to 0.3wt.%, a great number of Al_3Fe particles are distributed on the fracture surface as marked by red arrows in Fig. 8(d). This reveals that the microcrack is generated at particles interface, which can be attributed to the lower ductility of Alloy 4. Therefore, the morphology of the Al_3Fe phase on the grain boundary has an important influence on the mechanical properties of the alloy.

Figures 9(a) and (b) show the morphology of the tensile fracture side of Alloy 1. It can be found that obvious micro-crack and porosities near the fracture, and the micro-cracks spread along the surrounding pores. Figures 9(c) and (d)

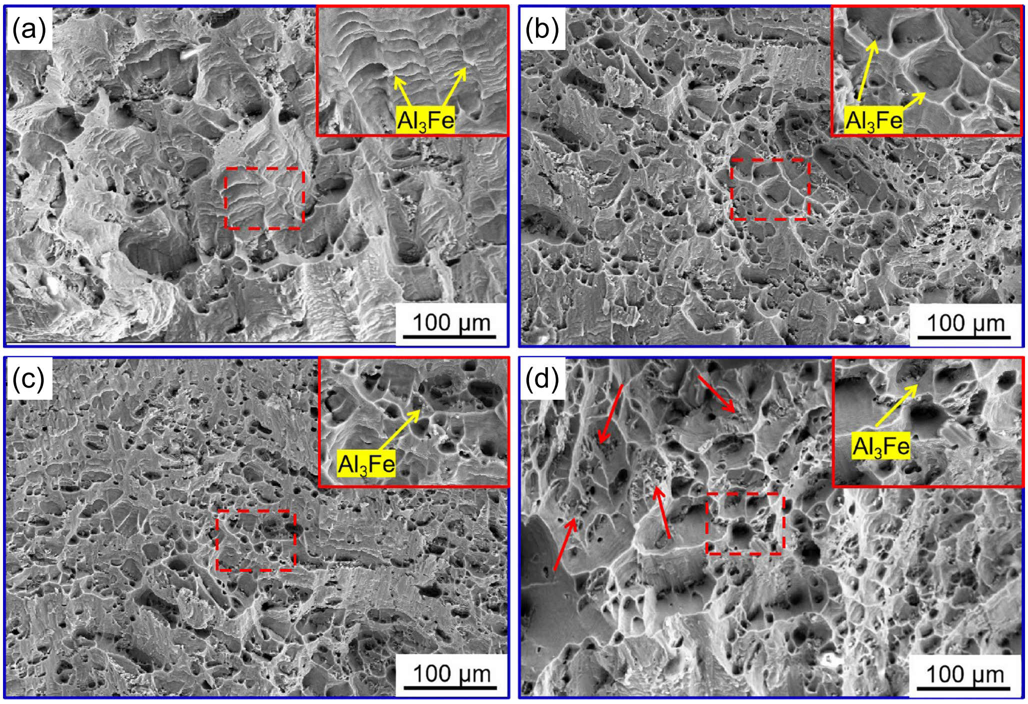

Fig. 8: SEM image of tensile fracture morphology: (a) Alloy 1; (b) Alloy 2; (c) Alloy 3; (d) Alloy 4

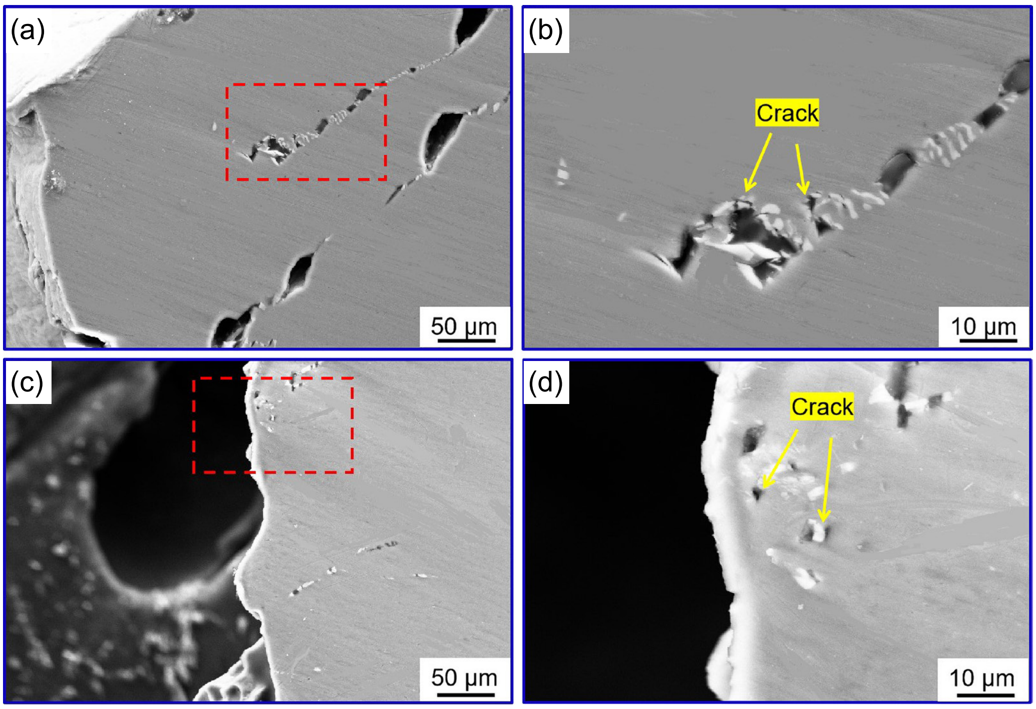

Fig. 9: SEM image of tensile fracture side of Alloy 1 (a–b) and Alloy 4 (c–d)

show the morphology of the tensile fracture side of Alloy 4. The Al_3Fe phase changes from needle-like shape into granular particles by adding Sc, and few microscopic cracks are produced in the granular Al_3Fe phase, which shows that the Al_3Fe phase morphology is the primary factor affecting the cracks. By adding different concentrations of Sc to the AA5052 aluminum alloy, the morphology of the Al_3Fe phase is changed to granular shape, thus, the mechanical properties of the alloy are improved and the hot cracking is eliminated.

In AA5052 aluminum alloy, Fe is a harmful element when it is present in the form of solid solution atoms or an iron-containing phase, and its existence has an adverse impact on the performance of the alloy [29]. The atomic radius of Fe is only 12% larger than that of Al, and the maximum equilibrium solid solubility of Fe in Al is only 0.052wt.%. Therefore, the solution strengthening effect of Fe in aluminum alloys is quite poor. The Fe content in this studied alloy is much greater than the maximum equilibrium solid solubility of Fe. Therefore, most of the Fe exists in the form of a second phase, the coarse needle-like Al_3Fe phase.

The Al_3Fe phase is present in a hundred-micron, needle-like form in Alloy 1. By adding 0.3wt.% Sc, the hundred-micron, needle-like Al_3Fe phase in the AA5052 alloy is transformed into several micron-sized, granular Al_3Fe phase, which increases the tensile strength of the alloy by 70 MPa. Therefore, when the needle-like Al_3Fe phase is changed to fine particles, it becomes a strengthening phase rather than a harmful phase, thus playing a role in improving strength of AA5052 aluminum alloys. The Al_3Fe phase is base-centered and monoclinic. Therefore, there are obvious differences between the Al_3Fe phase and Al in structure and lattice parameters. When the Al_3Fe phase in aluminum alloys is nano-sized, it becomes a strengthening phase. The strengthening of the nano-sized Al_3Fe phase is caused by the Orowan dislocation bypass mechanism [30]. A smaller average particle radius can obtain a better strengthening effect [31].

4 Conclusions

(1) In AA5052 aluminum alloy, the addition of Sc can change the morphology of the Al_3Fe phase. When Sc is not added, the Al_3Fe phase is thick and needle-like, with a size of approximately 100 μm. When 0.3% Sc is added, the Al_3Fe phase becomes nearly spherical with a size of approximately 2 μm.

(2) The addition of Sc into AA5052 aluminum alloy can effectively refine the average grain size, and decrease the proportion of LAGBs.

(3) The average tensile strength of the AA5052 aluminum alloy prepared by adding different contents of Sc (0, 0.05%, 0.2%, and 0.3%) is 181 MPa, 196 MPa, 216 MPa, and 251 MPa, respectively, the addition of 0.3% Sc increases the tensile strength by 70 MPa, indicating that Sc can effectively improve the strength of the alloy. But the average elongation after fracture is 19.8%, 30%, 23.5%, and 19.3%, respectively, which is noticeably increased due to the morphology change of the Al_3Fe phase from needle-like to spherical and then decrease because of significant increases in HAGBs with the increase of Sc.

Acknowledgments

This work was financially supported by the Key Research & Development Program of Yunnan Province (Grant numbers 202103AA080017 and 202203AE140011).

Conflict of interest

The authors declare that they have no known competing financial interests or personal relationships that could have appeared to influence the work reported in this paper.

References

[1] Zha M, Li Y J, Mathiesen R H, et al. Microstructure evolution and mechanical behavior of a binary Al-7Mg alloy processed by equal-channel angular pressing. Acta Materialia, 2015, 84: 42–54.

[2] Fazeli F, Poole W J, Sinclair C W. Modeling the effect of Al_3Sc precipitates on the yield stress and work hardening of an Al-Mg-Sc alloy. Acta Materialia, 2008, 56(9): 1909–1918.

[3] Guan R G, Shen Y F, Zhao Z Y, et al. A high-strength, ductile Al-0.35Sc-0.2Zr alloy with good electrical conductivity strengthened by coherent nanosized-precipitates. Journal of Materials Science & Technology, 2017, 33(3): 215–223.

[4] Singh V, Prasad K S, Gokhale A A. Microstructure and age hardening response of cast Al-Mg-Sc-Zr alloys. Journal of Materials Science, 2004, 39(8): 2861–2864.

[5] Zhang P, Li Z M, Liu B L, et al. Tensile properties and deformation behaviors of a new aluminum alloy for high pressure die casting. Journal of Materials Science & Technology, 2016, 33(4): 367–378.

[6] Wang B, Chen X H, Pan F S, et al. Effects of cold rolling and heat treatment on microstructure and mechanical properties of AA 5052 aluminum alloy. Transactions of Nonferrous Metals Society of China, 2015, 25(8): 2481–2489.

[7] Moldovan P, Popescu G, Miculescu F. Microscopic study regarding the microstructure evolution of the 8006 alloy in the plastic deformation process. Journal of Materials Processing Technology, 2004, 153: 408–415.

[8] Sungjae W, Hyeongsub S, Jungwoo H, et al. Effects of Sc and Be microalloying elements on mechanical properties of Al-Zn-Mg-Cu (Al7xxx) alloy. Metals, 2023, 13(2): 340–340.

[9] Jiang H T, Xing H, Xu Z H, et al. Effect of Zn content and Sc, Zr addition on microstructure and mechanical properties of Al-Zn-Mg-Cu alloys. Journal of Alloys and Compounds, 2023, 947: 169246.

[10] Benarieb I, Dynin N, Zaitsev D V, et al. The structure and properties of wrought Al-Mg-Sc aluminum alloys with different scandiu. Physics of Metals and Metallography, 2023, 124: 65–73.

[11] Cai Y P, Su Y S, Liu K, et al. Effect of Sc microalloying on fabrication, microstructure and mechanical properties of SiC_p/Al-Cu-Mg-Sc composites via powder metallurgy. Materials Science & Engineering: A, 2023, 877: 145152.

[12] Zhao Z H, Meng Y, Cui J Z. Effect of Mn on microstructures and mechanical properties of Al-Mg-Si-Cu-Cr-V alloy. China Foundry, 2012, 9(4): 349–355.

[13] He Y D, Zhang X M, Cao Z Q. Effect of minor Sc and Zr addition on grain refinement of as-cast Al-Zn-Mg-Cu alloys. China Foundry, 2009, 6(3): 214–218.
[14] Zhang W W, Lin B, Fan J L, et al. Microstructures and mechanical properties of heat-treated Al-5.0Cu-0.5Fe squeeze cast alloys with different Mn/Fe ratio. Materials Science & Engineering: A, 2013, 588: 366–375.
[15] Qiu Y C, Yang X F, Xu J Y, et al. Enhanced mechanical property and corrosion resistance of alloy 5182 FSW joints by Sc and Zr alloying. Materials Characterization, 2022, 194: 112412.
[16] Ding R, Deng J W, Liu X C, et al. Enhanced mechanical properties and thermal stability in additively manufactured Al-Ni alloy by Sc addition. Journal of Alloys and Compounds, 2023, 934: 167894.
[17] Ostash O P, Polyvoda S L, Chepil R V, et al. Influence of rare-earth metals on the structure and properties of cast and deformed alloys of the Al-Mg-Cr-Sc-Zr system. Materials Science, 2022, 57(6): 846–857.
[18] Zhao J W, Guo A, Li H, et al. Semisolid slurry of 7A04 aluminum alloy prepared by electromagnetic stirring and Sc, Zr additions. China Foundry, 2017, 14(3): 188–193.
[19] Hou S H, Feng J, Chen S, et al. Effect of Ti, Sc and Zr additions on microstructure and mechanical properties of rheo-diecasting Al-6Zn-2Mg-2Cu alloys. China Foundry, 2023, 20(2): 125–133.
[20] Tang Z Q, Liu N, Su Y, et al. Effect of scandium on microstructure and properties of 6066 aluminum alloy and its aging process. Heat Treatment, 2016, 31(1): 7–10. (In Chinese)
[21] Li B, Pan Q L, Shi Y J, et al. Microstructural evolution of Al-Zn-Mg-Zr alloy with trace amount of Sc during homogenization treatment. Transactions of Nonferrous Metals Society of China, 2013, 23(12): 3568–3574.
[22] Wang Y X, Wu G H, Zhang L, et al. Enhanced strength and ductility in sand-cast Al-Li-Cu-Mg-Zr alloy via synergistic microalloying with Sc and Ti. Journal of Alloys and Compounds, 2023, 962: 170954.
[23] Patakham U, Kajornchaiyakul J, Limmaneevichitr C. Grain refinement mechanism in an Al-Si-Mg alloy with scandium. Journal of Alloys and Compounds, 2012, 542: 177–186.
[24] Norman A F, Prangnell P B, Mcewen R S. The solidification behaviour of dilute aluminium-scandium alloys. Acta Materialia, 1998, 46(16): 5715–5732.
[25] Zhang M S, Wang J S, Wang B, et al. Quantifying the effects of Sc and Ag on the microstructure and mechanical properties of Al-Cu alloys. Materials Science & Engineering: A, 2022, 831: 142355.
[26] Zhu C, Zhao Z H, Wang G S, et al. Effect of 2024 Al alloy insert on the grain refinement of a 2024 Al alloy prepared via insert mold casting. Metals, 2019, 9(10): 1126.
[27] Zhang L C, Gu Y J, Xiang Y. Energy of low angle grain boundaries based on continuum dislocation structure. Acta Materialia, 2017, 126: 11–24.
[28] Liu B, Eisenlohr P, Roters F, et al. Simulation of dislocation penetration through a general low-angle grain boundary. Acta Materialia, 2012, 60(13–14): 5380–5390.
[29] Marzena L G, Sonia B. Iron phases in model Al-Mg-Si-Cu alloys. Materials Science Forum, 2011, 1205(674): 135–140.
[30] Yang Q, Bu F Q, Qiu X, et al. Strengthening effect of nano-scale precipitates in a die-cast Mg-4Al-5.6Sm-0.3Mn alloy. Journal of Alloys and Compounds, 2016, 665: 240–250.
[31] Fan Y Y, Makhlouf M M. Precipitation strengthening in aluminum-zirconium-vanadium alloys. Journal of Alloys and Compounds, 2017, 725: 171–180.